Scientia Iranica B (2015) 22(2), 423–435

SCIENTIA IRANICA

Sharif University of Technology
Scientia Iranica
Transactions B: Mechanical Engineering
www.scientiairanica.com

Hemodynamic analysis of pulsatile blood flow in a complete bypass graft with different anastomosis angles

E. Zohravi[a], E. Shirani[b,*] and M.R. Sadeghi[c]

a. *Department of Mechanical Engineering, Isfahan University of Technology, Isfahan, P.O. Box 8415683111, Iran.*
b. *Foolad Institute of Technology, Fooladshahr, Isfahan, P.O. Box 8491663763, Iran.*
c. *Department of Biomedical Engineering, University of Isfahan, Isfahan, P.O. Box 8174673441, Iran.*

Received 30 September 2012; received in revised form 6 August 2014; accepted 18 August 2014

KEYWORDS
Femoral bypass;
Hemodynamic;
Intimal hyperplasia;
Numerical simulation;
Bypass graft angle.

Abstract. The fluid flow through a bypass graft of 100% stenosed artery can substantially influence the outcome of bypass surgery. To help improve our understanding of this and related issues, unsteady flows for Newtonian/non-Newtonian fluids using Carreau's shear thinning model are numerically simulated in an arterial bypass system with complete occluded host artery. The objective of this study is to deal with the influence of the non-Newtonian property of fluid, effect of different bypass-host artery angle θ, and flow pulsatility on flow configuration, Wall Shear Stress (WSS), Oscillatory Shear Index (OSI), and flow phenomena during the pulse cycle. Here we use $\theta = 30°$, $45°$, $60°$ and $75°$ to study the effect of geometry. It is found that θ has strong influence on hemodynamic in distal femoral artery anastomoses. Results show that a bypass femoral anastomosis with a moderate θ, like $\theta = 45°$, enhances its long-term performance. Also, significant difference between the non-Newtonian and Newtonian pulsatile flows is revealed. This shows the necessity of using non-Newtonian model rather than Newtonian model for such flows. The unsteadiness of flow using the femoral pulse shows complex flow characteristics, and requires the use of unsteady analysis.

1. Introduction

Occlusion of arteries due to the atherosclerotic plaque formation is the leading cause of mortality in developed countries [1]. In recent years, surgical treatments of cardiovascular diseases have developed rapidly, and Coronary Artery Bypass Grafting (CABG) has been widely used for patients with severe coronary artery diseases. However, up to 25% of the grafts become occluded in one year and up to 50% occluded in ten years [2]. Intimal hyperplasia which is related to distribution of Wall Shear Stress (WSS) is an important factor related to the failure of the coronary bypass surgery. The feature of the WSS is associated with the development of the intimal hyperplasia on the native artery bed. In general, atherosclerotic lesions in the coronary arteries are related to low and oscillating wall shear stress [3]. Once the magnitude of the wall shear stress exceeds 400 dynes/cm^2, the endothelium surface is irreversibly damaged [4]. Also a number of studies suggested that most intimal thickening, IT, occurs where the mean WSS is less than about 10 dynes/cm^2 [5,6].

Hemodynamic is thought to play an important role for the localization of vascular disease in areas of complex flow in the coronary, carotid, and femoral arteries. These complex flow regions often occur due to branching, bifurcation, and curvature of the arteries. A variety of hemodynamic factors have been implicated in the development of atherosclerosis, including disturbed flow patterns [7,8], low shear stress [9-11], low and

*. *Corresponding author. Mobile: +98 913 1671350*
E-mail address: eshirani@cc.iut.ac.ir (E. Shirani)

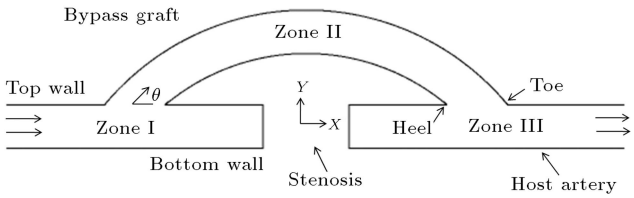

Figure 1. The geometric configuration of the model arterial bypass system.

oscillating shear [12-14] temporal variation of the shear stress [15] and spatial wall shear stress gradient [16,17]. Meanwhile, it is noted that there exist three risk factors for the development of atherogenesis [18], which include low shear stress region, high vessel pressure distribution, and high particle residence time in the region of atherosclerosis.

However, most of these reports do not consider the effect of the non-Newtonian property of blood and effect of angle θ on hemodynamic (shown in Figure 1), in complete bypass. Although the assumption of Newtonian behavior of blood is acceptable for high shear-rate flow, it is not valid for low shear-rate regions (less than 100 s), such as downstream of stenosis [19]. In this study, we apply both Newtonian and non-Newtonian Carreau fluid model into complete bypass graft of femoral artery with 100% stenosis using four different angles θ between bypass and host artery. We focus our attention on their effects on some hemodynamic parameters, such as flow configuration, WSS, OSI, and secondary flow, in the host artery and bypass.

2. Governing equations

In this study, we simulate the unsteady Newtonian and non-Newtonian blood flows in a 100% stenosed femoral artery and its bypass graft. Three-dimensional Navier-Stokes equations coupled with a non-Newtonian model are solved numerically using the finite volume-finite element based method. Effects of different bypass anastomotic angles, $\theta = 30°$, $45°$, $60°$, and $75°$, on the flow pattern are investigated.

Human blood is modeled as an incompressible Newtonian and non-Newtonian fluid and its flow in the artery is assumed to be mainly laminar. The governing equations consist of the continuity and Navier-Stokes equations:

$$\nabla.\mathbf{u} = 0, \tag{1}$$

$$\frac{\partial \mathbf{u}}{\partial t} + \mathbf{u}\nabla.\mathbf{u} = \frac{1}{\rho}\nabla.\boldsymbol{\sigma}, \tag{2}$$

where $\mathbf{u}$ denotes the blood velocity vector, ρ is the density of blood, σ is the total stress tensor which is related to the pressure p and shear stress $\boldsymbol{\tau}$ by $\boldsymbol{\sigma} = -pI + \boldsymbol{\tau}$. The shear stress tensor depends on the rate of deformation tensor $\mathbf{D}$ by $\boldsymbol{\tau} = 2\eta(\dot{\gamma})\mathbf{D}$, in which $\mathbf{D} = 1/2(\nabla\mathbf{u} + \nabla\mathbf{u}^T)$, η and $\dot{\gamma}$ denote the viscosity of blood and shear rate, respectively. The viscosity of blood η has been found to depend on the shear rate $\dot{\gamma}$ and various models have been proposed to describe the relation between η and $\dot{\gamma}$. In this work, we use Carreau's shear thinning model [20]:

$$\eta = \eta_\infty + (\eta_0 - \eta_\infty)\left[1 + (\lambda\dot{\gamma})^2\right]^{(n-1)/2}, \tag{3}$$

where $\dot{\gamma} = \sqrt{2tr(\mathbf{D}^2)}$ is a scalar measure of the rate of deformation tensor, η_0 and η_∞ denoting the zero shear viscosity and the infinite shear viscosity, respectively. The consistency index, n, is a parameter between 0 and 1. Based on Cho and Kensey [20], the above mentioned parameters have the typical values of $\eta_\infty = 0.0345$ gcm^{-1}s^{-1}, $\eta_0 = 0.56$ gcm^{-1}s^{-1}, $n = 0.3568$ and $\lambda = 3.313$ s.

3. Geometry and boundary conditions

The geometric configuration used in this work is shown in Figure 1 [21]. The origin is set at the XY symmetric plane (because of the symmetry with respect to the XY plane we consider only half of the flow field). Angle θ is measured from the line that connects the zenith of the curved bypass and the center of the curvature. The diameters of the bypass and the host tube are set equal. The host artery diameter varies from person to person and location to location, but here it is assumed to be 1 cm.

The distance between the heel and toe, shown in Figure 1, changes according to θ. The axial distance between entrance of host artery and bifurcating location is $24R$. The host artery outlet extended $50R$ in distance from toe. The extension between the ends of the host artery minimizes the effect of different inlet and outlet boundary conditions on the flow field near the bifurcation junction.

The origin of bypass $X/R = 0$ is set at the center of the fully occluded artery. The occlusion is represented by removing the corresponding part from the host artery. The location of the occlusion in the host tube is fixed and the cross span between the junctions is fixed at $16R$ in all cases. The occlusion length is $4R$. The arterial wall is assumed to be rigid.

For a typical femoral artery bypass grafting system, the boundary of the computation region consists of four parts, namely the inflow, symmetry plane, the artery wall, and the outflow boundary. The parabolic velocity distributions are set at the host arterial entrance:

$$u(r,t) = 2\overline{u}(t) * \left(1 - \left(\frac{r}{R}\right)^2\right). \tag{4}$$

At the inflow, the velocity is set based on the pulsatile

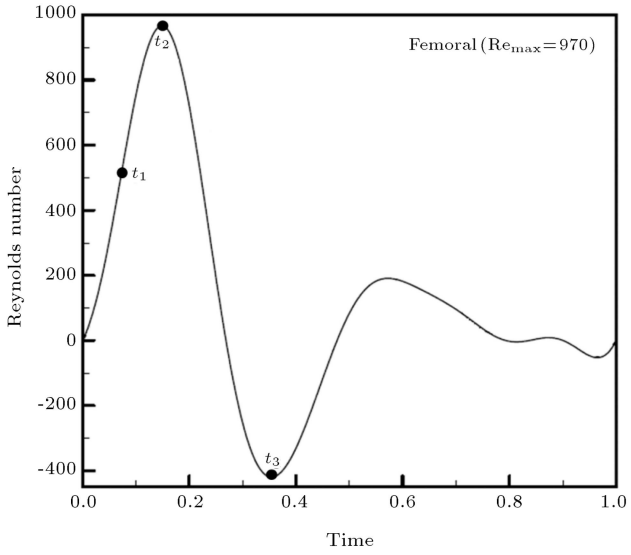

Figure 2. Flow waveform used in unsteady flow simulations.

velocity. The time-dependent simulation used a mid-femoral flow waveform given by Steinman [22], as depicted in Figure 2. The waveform is divided into 200 time steps, and results from the third cardiac cycle are extracted to eliminate the start-up effects of transient flow. During the reverse flow portion of the waveform, Re is negative. Therefore the numerical stability is enhanced by setting opening boundary condition at the outlet. On the arterial walls, no-slip conditions are applied.

4. Numerical method

The models are built up by ANSYS workbench software first, and then ANSYS CFX 11 is used to construct the mesh system and perform the numerical transition solutions. In the equations, the transient terms are modeled by a second-order backward scheme. The convergence tolerance is set as RMS of mass, and three velocity components are less than 1×10^{-4}.

5. Validation of numerical results

In order to validate our numerical results, we have simulated a typical test problem; the flow in an end-to-side anastomosis. The majority of studies on arterial bypass have been focused on this particular section because it is the site that restenosis is prone to occur. The test problem studied is a three-dimensional (3-D) rigid-wall model of an end-to-side anastomosis consisting of two cylindrical conduits of equal diameters intersecting at 45°. This flow configuration has been investigated by many researchers such as experimental work of Ojha et al. [23], and numerical simulations by Ethier et al. [24]. The configuration adopted is depicted in Figure 3. The coordinate scale is normalized by the tube diameter and

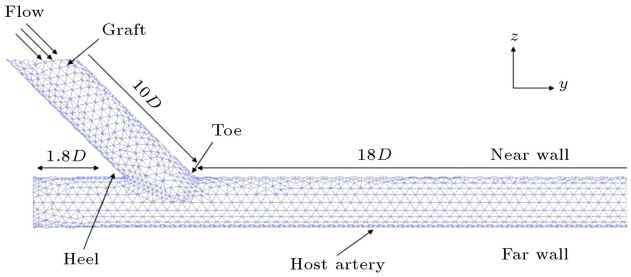

Figure 3. End-to-side arterial anastomosis model.

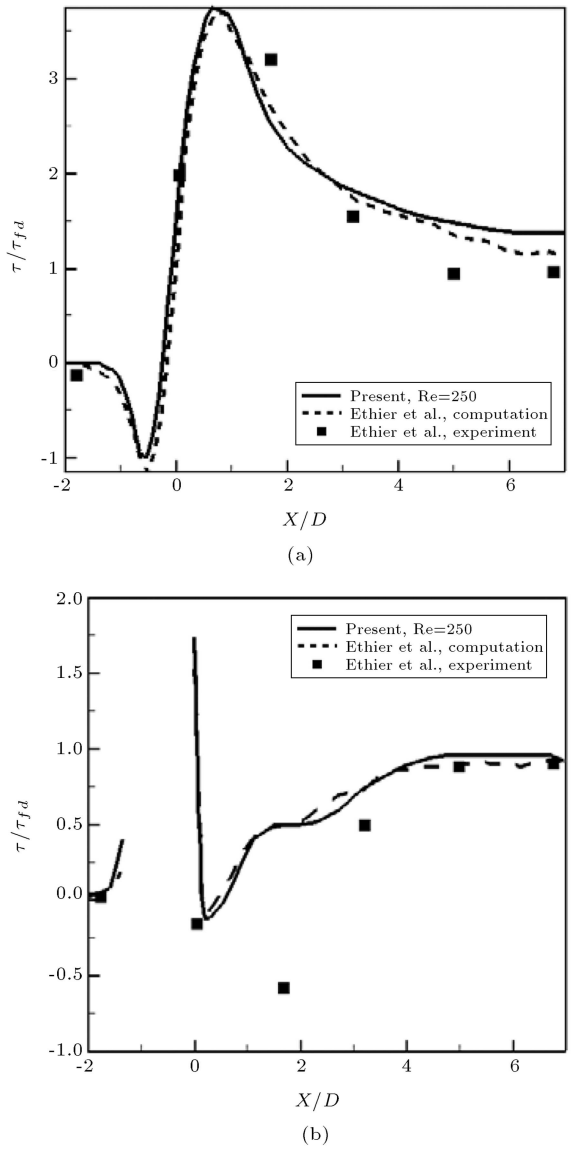

Figure 4. Validation of the numerical method by dimensionless WSS in: (a) Far wall, and (b) near wall of an end-to-side anastomosis.

is located at the toe. In Figure 4, the normalized axial variations of Wall Shear Stress (WSS), τ, along the far wall and near wall of the host artery are compared to the numerical simulations and experimental results obtained by Ethier et al. [24] for $Re = 250$. τ was

normalized by the corresponding Hagen-Poiseuille tube flow value under identical flow rate. Our results show good agreement with the numerical and experimental results by Ethier et al. [24].

6. Results and discussion

Blood flow in arteries is substantially influenced by unsteady flow phenomena. Time-dependent investigations are essential to reveal the dynamic behavior associated with pulsatile flows. Hence, in the following sections, results are shown at various times during the femoral pulsatile cycle. These times correspond to the mid-acceleration of systolic flow, t_1, peak of systolic flow, t_2, and peak of reverse flow, t_3, as shown in Figure 2.

Our attention is focused on the flow patterns, reverse flow, wall shear stress distributions, OSI and secondary flows. Also we compare these parameters for different anastomotic angles and Newtonian/non-Newtonian models.

6.1. Flow configuration

In this section, the effect of angle, θ, on flow configuration is investigated. To do this, since at $t = t_2$ the flow rate is maximum and the flow separation zone is more pronounced, the flow configurations are shown at this time. Here results for non-Newtonian model are shown. The flow configuration does not reveal so many differences for Newtonian and non-Newtonian model. In the next sections the difference will be considered by presenting other parameters. Figure 5 shows the velocity profiles on the symmetric plane for four angle θ at t_2 and for non-Newtonian model.

The results show that in zone I, the flow patterns are similar for all angles, except that as θ increases due to the sudden change in flow direction and a smaller bifurcation junction area, the shear stresses around the tuning corner become larger. In the downstream half of the bypass, the velocity profile tends to move closer to the outer wall owing to a larger curvature resulted from a larger θ, leading to a higher shear rate at the toe. In zone III, the reduced flow velocity on the symmetric plane downstream of the anastomosis indicates a stronger helical flow structure for larger θ.

Figure 6 shows the reverse flows on the symmetric plane for four angle θ in zone III at t_2 and for non-Newtonian model. Since the distal anastomosis junction is of particular interests, most of the following results are presented in zone III.

The reverse flow regions, shown in Figure 6, also suggest a positive correlation of the size of recirculation zones, both in the bottom wall after the stenosis and near the toe, with the anastomotic angle. In this figure numbers 1 to 9 indicate the size of the reverse flow velocity.

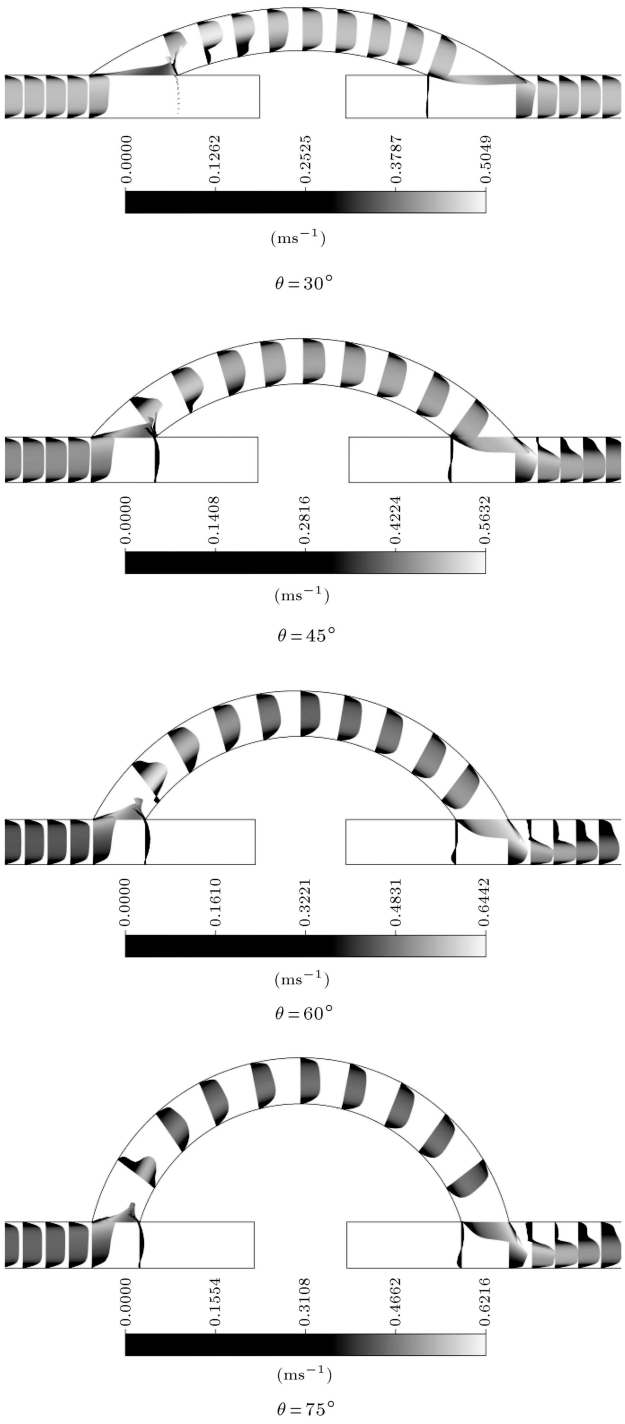

Figure 5. The velocity profiles on the symmetric plane at t_2 and non-Newtonian model.

6.2. Wall Shear Stress (WSS)

Shear stress is an important indicator for the hemodynamic influences on the vessel walls. Distributions of WSS in zone III along the top wall (immediately after the toe) and the bottom wall (after the stenosis) for four angle θ are shown in Figures 7-9, at three times of t_1, t_2 and t_3.

The results exhibit that there exists significant

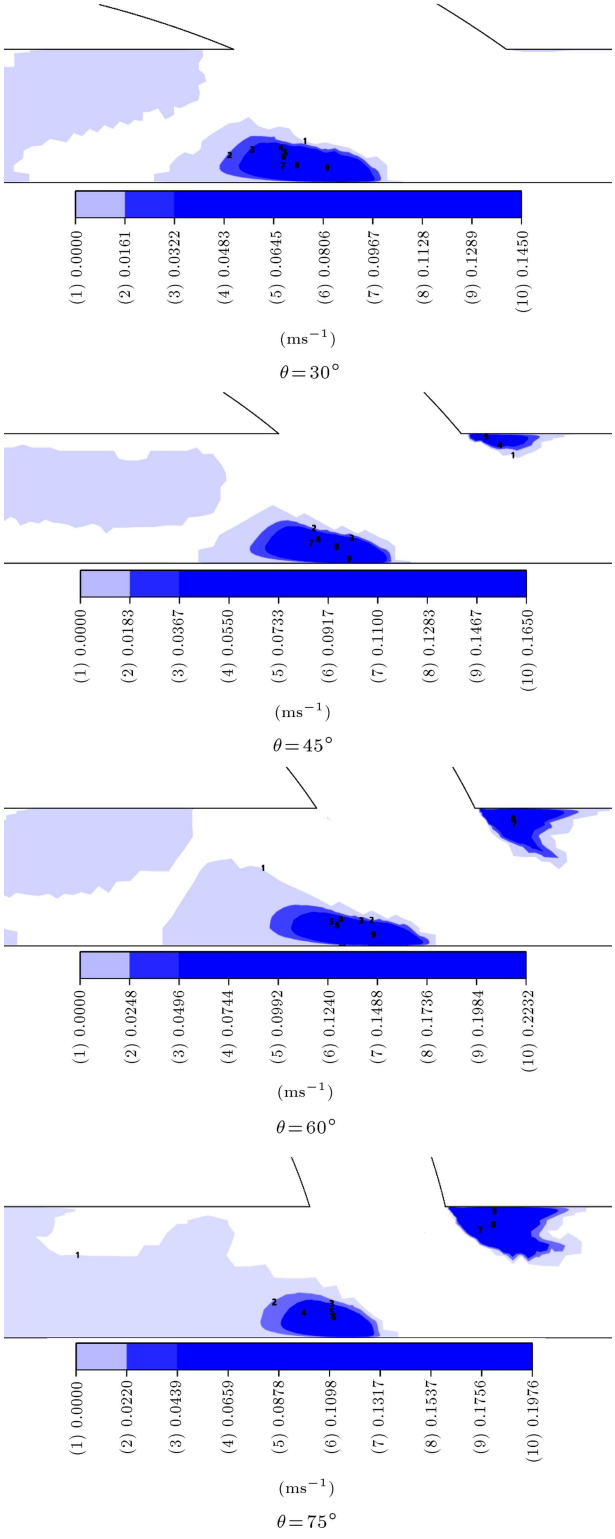

Figure 6. The reverse flow on the symmetric plane in zone III at t_2 and non-Newtonian model.

difference between values of WSS for non-Newtonian and Newtonian flows. Higher absolute values of WSS are observed for the non-Newtonian flow for all cases. It is found that for high values of velocities and so WSSs, there is not any significant difference between these two models. For example at t_2 this difference is less than those at t_1 and t_3. Because of low values of WSS at $t1$, where the blood behaves like non-Newtonian flow, this difference is more pronounced.

As the mean inlet velocity reaches its maximum value and the viscous boundary layer becomes much thinner at peak of systolic flow, t_2, the magnitudes of WSS are larger compared to WSS at t_1 and t_3 at both top and bottom walls.

The intensity of the reverse flow next to the occlusion enhanced with increasing inlet Re (recognized by the WSS values within the region) at t_2 comparing with t_1. The WSS along the top wall shows that the size and strength of the recirculation zone immediately after the toe augments with inlet Re.

The peak of WSS on the bottom wall that happens opposite of the toe increases with increasing the angle θ. Then the results show that the location near the toe on the top wall and opposite of the toe and heel on the bottom wall are sensitive sites. For t_1 and t_2 the length and strength of recirculation zone increase with increasing angle θ on the top wall.

For peak of reverse flow, Figure 9, the absolute value of WSS at the toe increases with increasing angle θ on the top wall. At t_3 the inlet velocity is negative, and the flow direction is reversed. On the top wall there are recirculation zones everywhere.

The results at all times show that when θ is smaller, WSS evolves more gradually and their peak values are smaller as well. Overall, a smaller angle provides smoother flow path and less flow disturbances, and, eliminates some recirculation zones. Nevertheless, when the angle is smaller, the interfacial area between the bypass tube and the host artery will be larger. This requires longer suture line, and will be more vulnerable to thrombosis. Thus, a better anastomotic angle might need more contemplation.

6.3. Oscillatory Shear Index (OSI)

$\vec{\tau}_w$ is defined by $\vec{\tau}_w = (\tau_x, \tau_y, \tau_z)$ where τ_x, τ_y and τ_z are the components of WSS in x, y, and z directions, respectively. The time-average WSS is defined as:

$$\overline{|\vec{\tau}_w|} = \frac{1}{T}\int_0^T |\vec{\tau}_w| dt, \tag{5}$$

where $|\vec{\tau}_w| = \sqrt{\tau_x^2 + \tau_y^2 + \tau_z^2}$ is the magnitude of transient WSS and T is the duration of one flow cycle. Eq. (6) is approximated by summing up the values of WSSs at 200 time steps in one cycle. OSI provides a good measure of cyclic variations of WSS in three-dimensional space. The definition used in this study is taken from [25]:

$$\text{OSI} = 0.5 * \left(1 - \frac{|\int_0^T \vec{\tau}_w dt|}{\int_0^T |\vec{\tau}_w| dt}\right). \tag{6}$$

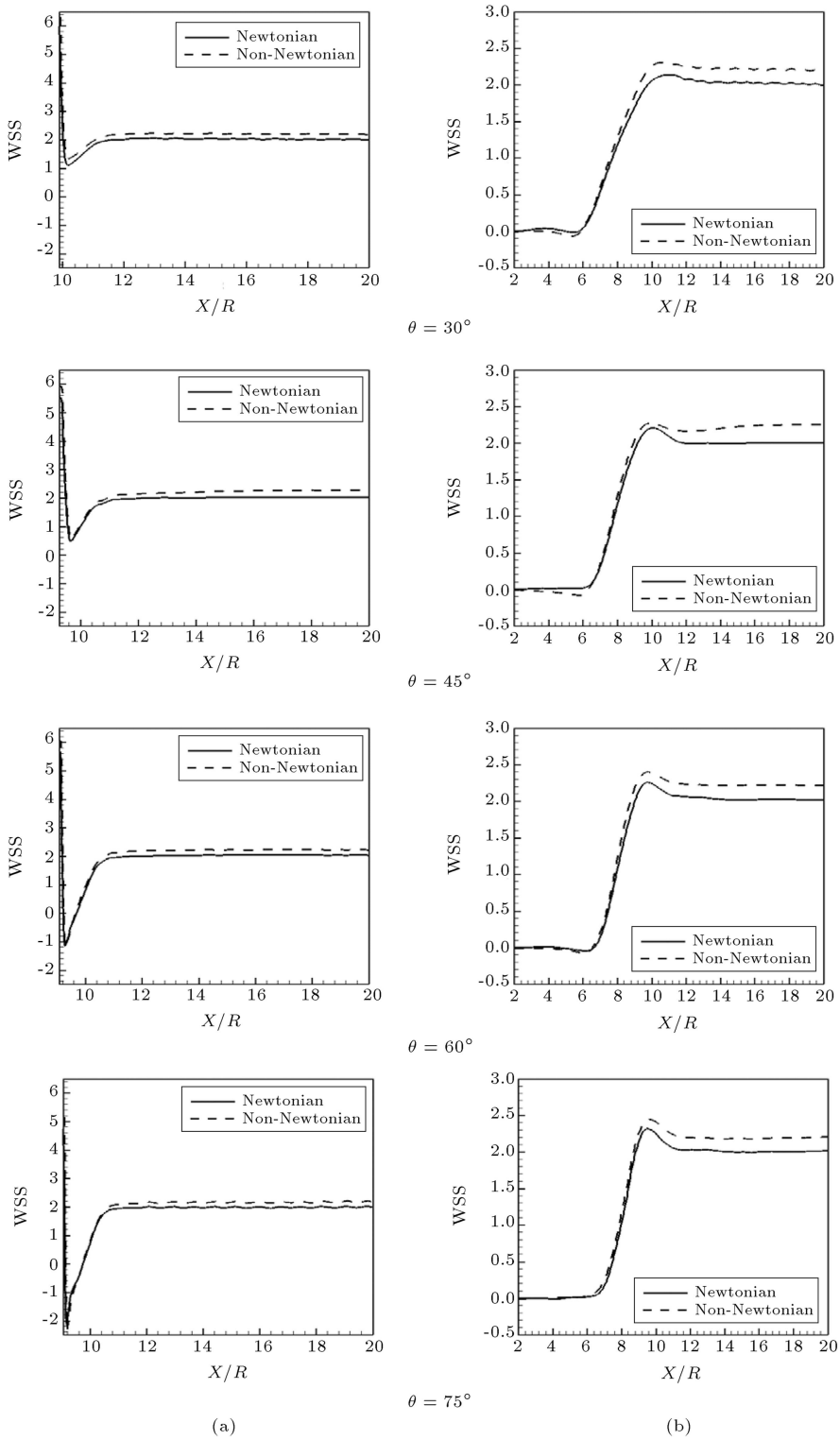

Figure 7. Distributions of WSS along the wall in zone III at the mid-acceleration of systolic flow, t_1, for Newtonian (solid line), non-Newtonian (dashed line) fluid flows: (a) Top wall; and (b) bottom wall.

The OSI value ranges from 0 to 0.5. Values of 0 and 0.5 correspond to completely and zero forward flow, respectively.

Distributions of OSI along the top and bottom walls in zone III and for four different θ values are shown Figure 10. In this figure, L on the top wall is a distance measured from the toe. Also L on the bottom wall is a distance along the wall from a point opposite of the heel. The peak of OSI, i.e.,high shear stress temporal oscillations, 0.5, along

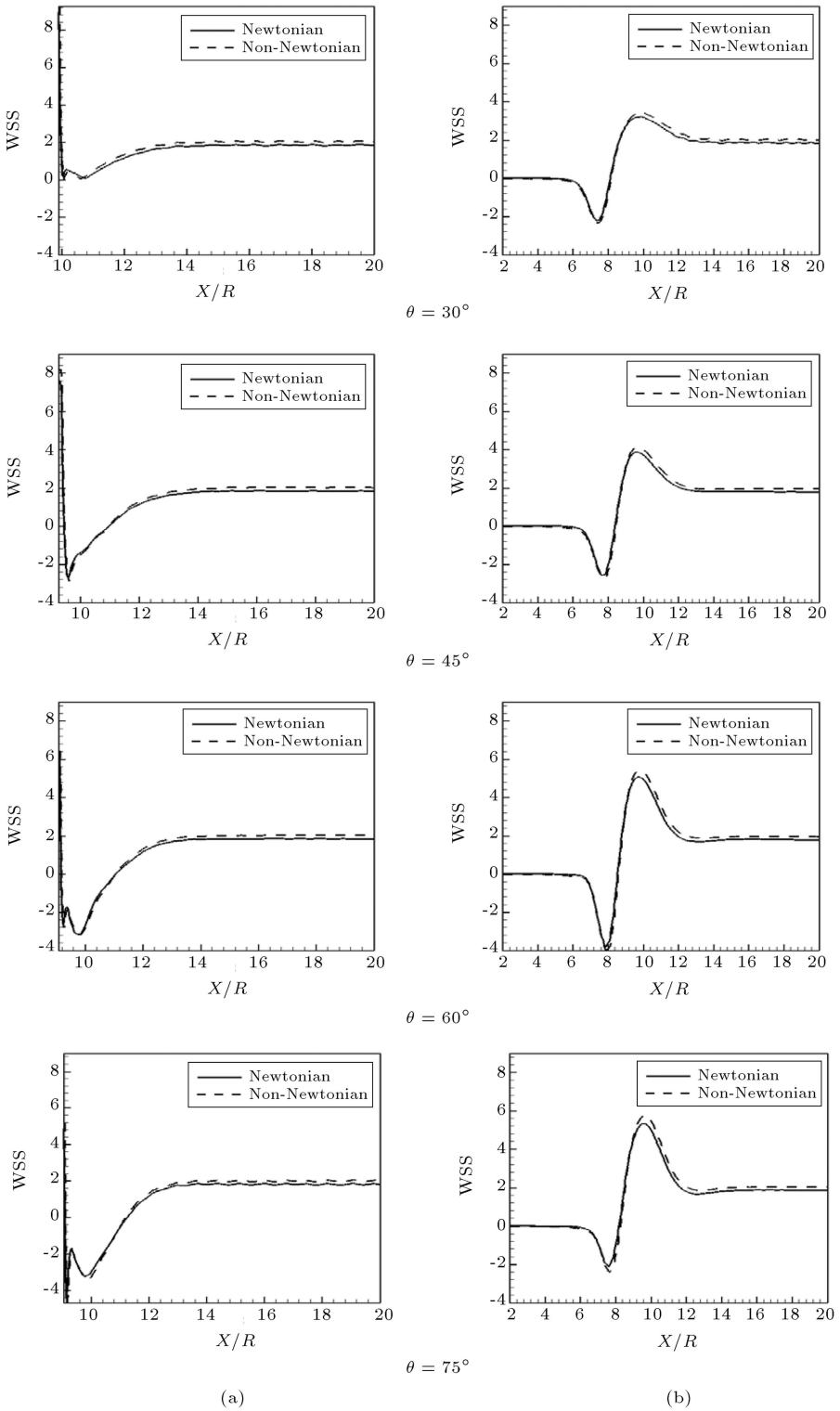

Figure 8. Distributions of WSS along the wall in zone III at the peak of systolic flow, t_2, for Newtonian (solid line), and non-Newtonian (dashed line) fluid flows: (a) Top wall; and (b) bottom wall.

the top for all four θ angles and bottom walls for $\theta = 30°$ and $45°$ are formed at two locations. One is immediately after the toe and another is about $3R$ after the toe, on top wall, and for the bottom wall, one occurs after the heel and another after the toe. For bottom wall and $\theta = 60°$ and $75°$, there is only one location with OSI=0.5 and its location is about $2R$ after the toe. The regions with high OSI closely resemble those with low WSS (Figures 7 to 9).

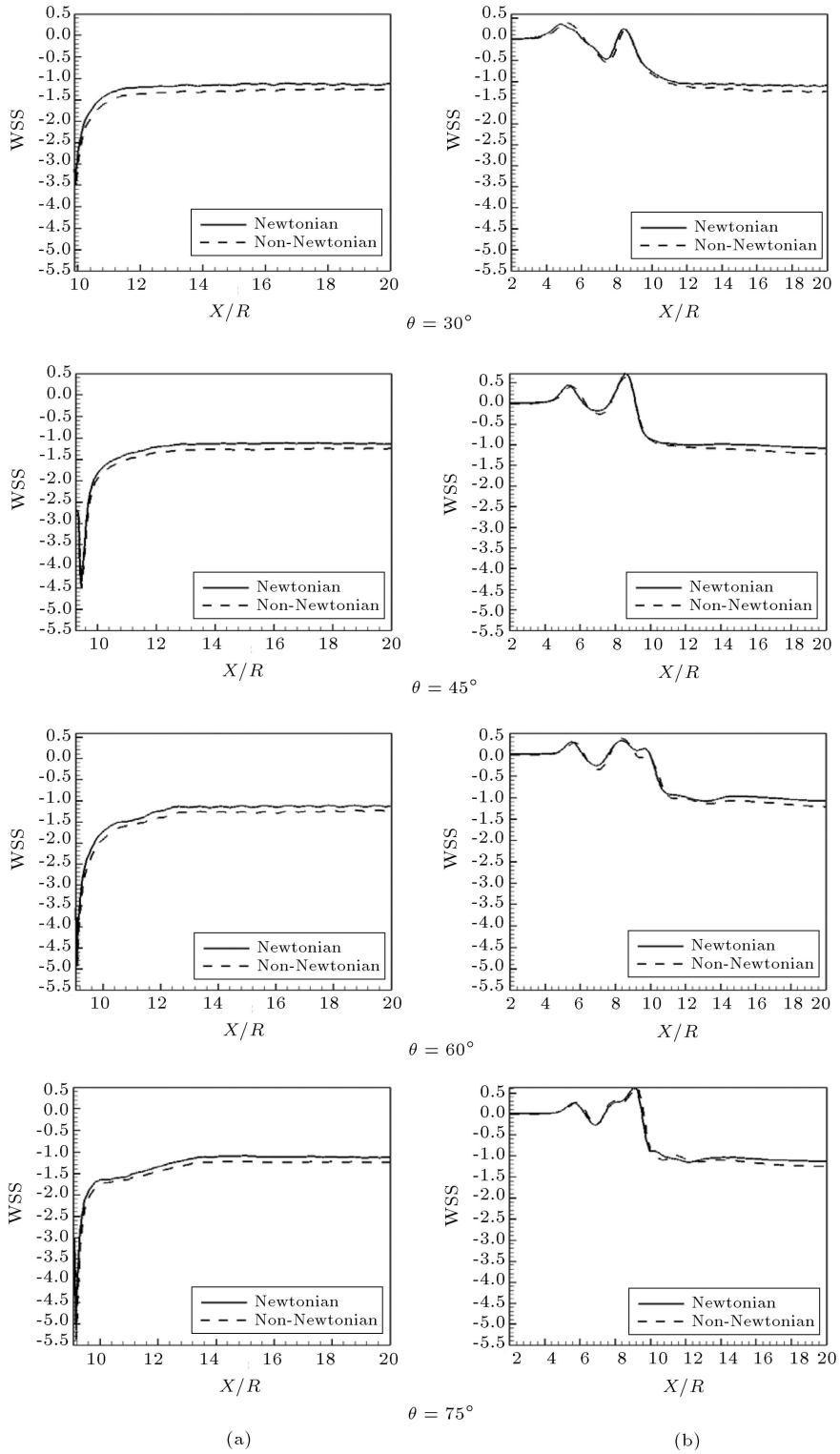

Figure 9. Distributions of WSS along the wall in zone III at the peak of reverse flow, t_3, for Newtonian (solid line), and non-Newtonian (dashed line) fluid flows: (a) Top wall; and (b) bottom wall.

Like WSS, the results exhibit a significant difference of OSI for non-Newtonian and Newtonian flows.

The distribution of OSI in zone III along the top and bottom walls shows that by increasing θ, OSI, tends to shift high values from the toe on the top wall and heel on the bottom wall to the region upstream of the toe, but the overall OSI levels for $\theta = 30°$, $45°$, $60°$ and $75°$ are comparable especially on the top wall. With increasing θ, the value of OSI decreases; regions with OSI=0.5 are reduced and high values of

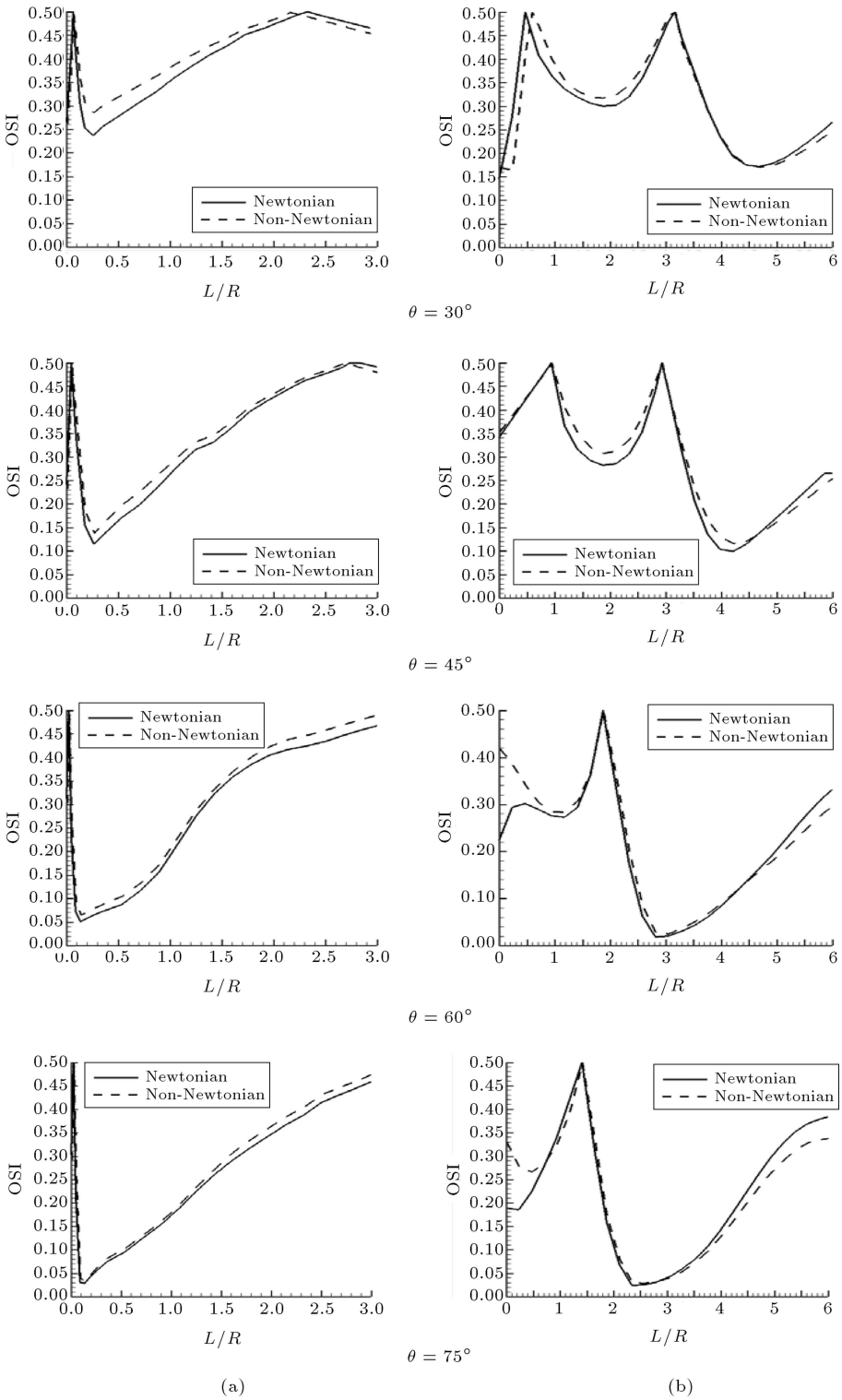

Figure 10. Distributions of OSI along the wall in zone III for Newtonian (solid line), and non-Newtonian (dashed line) fluid flows: (a) Top wall; and (b) bottom wall.

OSI tend to shift from toe. Regarding the value of OSI, increasing θ is useful. This result is opposite of results that we deduced from WSS. As shown before, values of WSS reduce with increasing θ.

The correlation between IT and sites with low WSS and particularly low OSI has been well documented [5,26]. Biological studies suggest that low WSS and high OSI stimulate intimal thickening. Low flow and low-shear magnitude may also increase surface concentration of Low-Density Lipoprotein (LDL), thus

promoting the rate of lipid infiltration into the blood vessel [27]. Although the lower threshold of mean WSS is still not definitive, a number of studies suggest that most IT occurs where mean WSS is less than about 10 dynes/cm^2 [5,6,26].

If θ is varied, apparently certain aspects of hemodynamic are changed. Generally, smaller θ is associated with higher OSI in the anastomotic region, whereas larger θ leads to higher SWSSG (Spatial Wall Shear Stress Gradient) on the host artery bed [28]. It is found that the smallest θ produced the least amount of flow skewing and thus SWSSG in the host artery bed [29]. However, no significant adverse effect is observed for small θ in their study. In another study for steady and pulsatile sinusoidal flows when $\theta = 15°$, $30°$ and $45°$ and $\Phi = 1 : 1$ (Φ=diameter ratio), pronounced flow separation and flow reversal region at the toe are extended several vessel diameters along the bed of the distal artery for $\theta = 30°$ and $45°$ [30]. These phenomena are not observed in our study. The discrepancies are probably due to a smaller Φ or higher flow rate (Re_m= 300 and 500) used in their flow visualization study. These factors would increase the momentum of the graft flow, and thus accentuate downstream flow skewing towards the artery bed and encourage flow separation at the toe. Consequently, smaller θ should be used in their studies compared to ours, to compensate the adverse effects of flow skewing and separation. Namely, for smaller Φ or higher flow rates, smaller θ should be adopted to inhibit the flow separation and reduce high shear rate gradient regions.

6.4. Secondary flow

Different features for the non-Newtonian and Newtonian fluid flows have been discussed in the previous section. To exhibit the influence of the bifurcation and curvature on the flow structure, the secondary flow field is further analyzed here. Figure 11 shows the velocity vectors in cross section of the artery at the toe for the non-Newtonian fluid at mid-acceleration of systolic flow, t_1, peak of systolic flow, t_2, and peak of reverse flow, t_3, respectively. In this figure, due to the symmetry, only half of the cross sections is shown.

The presence of the secondary flow is caused by a centripetal acceleration (or pressure gradient) introduced by the curvature in the bypass. At section close to the bifurcation, the counter-rotating vortices (i.e., Dean Vortices) are evident and result a shift of the peak axial velocity toward the top wall during the cycle. The secondary vortex at t_2, shown in Figure 11(b), exhibits essentially different features as that at the peak of reverse flow in Figure 11(c). At the peak of systolic flow, the secondary vortex is formed near to the wall but at the peak of reverse flow, it is near the center of vessel. The strength of the Dean vortex at the peak of systolic flow shown in Figure 11(b), compared to that shown in Figure 11(a) for the mid-acceleration of systolic flow, increases. As shown in Figure 11(a)-(c), all vortices move counterclockwise. The reverse flow regions shown in Figure 11 also suggest a correlation of the size of recirculation zones, near the toe with θ.

7. Conclusion

The underlying doctrine of this study is to set up a numerical platform to facilitate preoperational planning of bypass surgery. One aspect of the arterial bypass hemodynamic presented is the flow pulsatility. The time-dependent computation using a femoral flow waveform clearly demonstrated the dynamic and complex flow behavior and therefore the necessity of using unsteady analysis. Results indicated that locations, where intimal hyperplasia has been reported to be prone to occur, are generally consistent with regions of low oscillating shear.

Overall, a smaller angle θ provides smoother flow path and less flow disturbances, and meanwhile, eliminates some recirculation zones under the applied flow condition. Nevertheless, when the angle is smaller, the interfacial area between the bypass tube and the host artery will be larger. This requires longer suture line, and will be more vulnerable to thrombosis. Also overall OSI levels show that with increasing θ, the overall OSI decreases. Thus a better anastomotic angle might need more contemplation. We recommend that a bypass femoral anastomosis with a moderate θ, like $\theta = 45°$ would enhance its long-term performance.

The significant difference between the non-Newtonian and Newtonian pulsatile flows is revealed at times where velocities are low and in regions near the toe on the top wall and opposite of the heel and toe on the bottom wall. But both models show similar trends for WSS and OSI with changing θ. The calculated results support the fact that blood behaves as non-Newtonian fluid and the assumption of Newtonian fluid for blood in this case may introduce some errors.

Acknowledgment

We thank the Department of Mechanical Engineering at Isfahan University of Technology of Iran for its support.

Conflict of interest

There are no financial and personal relationships with other people or organizations that could inappropriately influence (bias) their work.

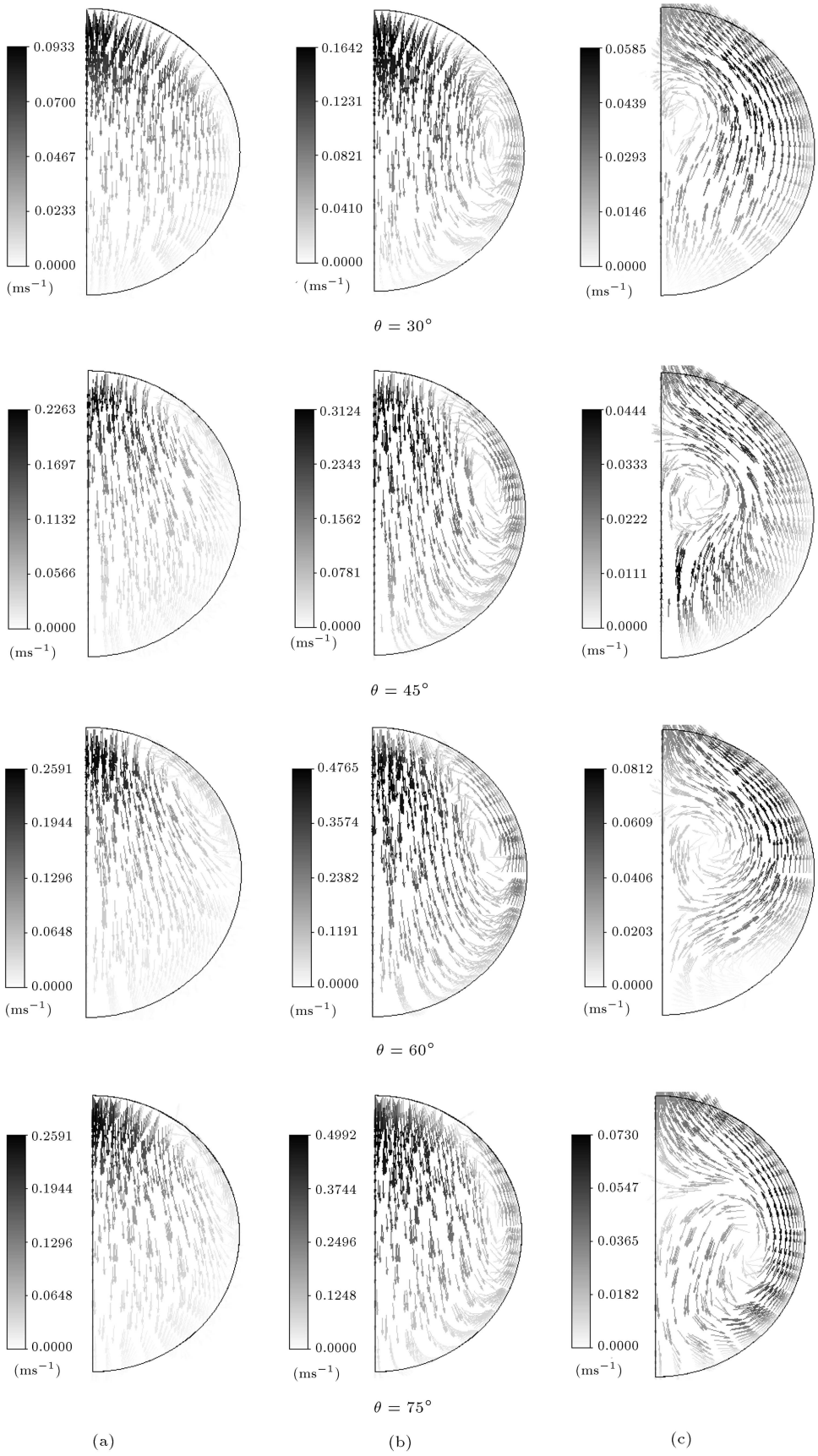

Figure 11. Secondary flow velocity vectors in the artery cross section at the toe for non-Newtonian fluid at: (a) t_1; (b) t_2; and (c) t_3.

References

1. Caro, C.G., Fitz-Gerald, J.M. and Scliroter, R.C. "Atheroma and arterial wall shear: Observation, correlation and proposal of a shear dependent mass transfer mechanism for atherogenesis", *Proc. Roy. Soc.*, **177**, pp. 109-33 (1971).
2. Papaharilaou, Y., Doorly, D.J. and Sherwin, S.J. "The influence of out-of plane geometry on pulsatile flow within a distal end-to-side anastomosis", *J. Biomech*, **35**, pp. 1225-39 (2002).
3. Weydahl, E.S. and Moore, JE. "Dynamic curvature strongly affects wall shear rates in a coronary artery bifurcation model", *J. Biomech*, **34**, pp. 1189-96 (2001).
4. Ku, D.N. "Blood flow in arteries", *Annu. Rev. Fluid Mech.*, **29**, pp. 399-434 (1997).
5. Ku, D.N., Giddens, D.P., Zarins, CK. and Glagov, S. "Pulsatile flow and atherosclerosis in the human carotid bifurcation positive correlation between plaque location and low oscillating shear stress", *Arterioscler Thromb. Vasc. Biol.*, **5**, pp. 293-302 (1985).
6. Kraiss, L.M., Kirkman, TR., Kohler, TR., Zierler, B. and Clowes, A.W. "Shear stress regulates smooth muscle proliferation and neointimal thickening in porous polytetrafluoroethylene grafts", *Arterioscler Thromb-Vasc Biol*, **11**, pp. 1844-52 (1991).
7. Hughes, P.E. and How, T.V. "Flow structures at the proximal side to-end anastomosis: influence of geometry and flow division", *Journal of Biomechanical Engineering*, **117**, pp. 224-36 (1995).
8. Staalsen, N.H., Vlrich, M., Winther, J., Pederson, E.M., How, T. and Nygaard, H. "The anastomosis angle does change the flow fields at vascular end-to-side anastomoses in vivo", *Journal of Vascular Surgery*, **21**, pp. 460-71 (1995).
9. Dobrin, P.B., Littooy, F.N. and Endean, E.D. "Mechanical factors predisposing to intimal hyperplasia and medial thickening in autogenous vein grafts", Surgery, **105**, pp. 393-400 (1989).
10. White, S.S., Zarins, C.K., Giddens, D.P., Bassiouny, H., Loth, F., Jones, S.A. and Glagov, S. "Hemodynamic patterns in two models of end-to-side vascular graft anastomoses: Effects of pulsatility, flow division, Reynolds number, and hood length", *Journal of Biomechanical Engineering*, **115**, pp. 104-11 (1993).
11. Delfino, A., Stergiopulos, N., Moore, J.E. and Meister, J.J. "Residual strain effects on the field in a thick wall finite element model of the human carotid bifurcation", *Journal of Biomechanics*, **30**, pp. 777-86 (1997).
12. Ene-Iordache, B., Cattaneo, L., Dubini, G. and Remuzzi, A. "Effect of anastomosis angle on the localization of disturbed flow in 'side-to-end' fistulae for haemodialysis access", Nephrol Dial Transplant, **28**, pp. 997-1005 (2013).
13. Sankaran, S., Esmaily-Moghadam, M., Kahn, AM., Guccione, J., Tseng, E. and Marsden, A.L. "Patient-specific multiscale modeling of blood flow for coronary artery bypass graft surgery", *Annals Biomed Eng.*, **40**(1), pp. 2228-2242 (2012).
14. Taylor, C.A., Hughes, T.J.R. and Zarins, C.K. "Effect of exercise on hemodynamic conditions in the abdominal aorta", *Journal of Vascular Surgery*, **29**, pp. 1077-89 (1999).
15. Kabinejadian, F., N.Ghista, D. "Compliant model of a coupled sequential coronary arterial bypass graft: Effects of vessel wall elasticity and non-Newtonian rheology on blood flow regime and hemodynamic parameters distribution", *Medical Engineering & Physics*, **34**(7), pp. 860-872 (2012).
16. Kleinstreuer, C., Lei, M. and Archie, J.P. "Flow input waveform effects on the temporal and spatial wall shear stress gradients in a new femoral graft-artery connector", *Journal of Biomechanical Engineering*, **118**, pp. 506-10 (1996).
17. Lei, M., Archie, J.P. and Kleinstreuer, C. "Computational design of a bypass graft that minimizes wall shear stress gradients in the region of the distal anastomosis", *Journal of Vascular Surgery*, **25**, pp. 637-46 (1997).
18. Araim, O., Chen, A.H. and Sumpio, B. "Hemodynamic forces: Effects on atherosclerosis", New Surgery, **1**, pp. 92-100 (2001).
19. Chien, S. "Hemorheology in clinical medicine", Clinical Hemorheology, **2**, pp. 137-42 (1982).
20. Cho, Y.I. and Kensey, R. "Effects of the non-Newtonian viscosity of blood flows in a diseased arterial vessel, Part 1: Steady flows", *Biorheology*, **28**, pp. 241-62 (1991).
21. Su, C.M., Lee, D., Tran-Son-Tay, R. and Shyy, W. "Fluid flow structure in arterial bypass anastomosis", *Journal of Biomechanics*, **127**, pp. 611-18 (2005).
22. Steinman, D.A., Vinh, B., Ethier, C.R., Ojha, M., Cobbold, R.S.C. and Johnston, K.W. "A numerical simulation of flow in a two-dimensional end-to-side anastomosis model", *ASME J. Biomech. Eng.*, **115**, pp. 112-18 (1993).
23. Ojha, M., Ethier, C.R., Johnston, K.W. and Cobbold, R.S.C. "Steady and pulsatile flow fields in an end-to-side arterial anastomosis model", *J. Vasc. Surg.*, **12**, pp. 747-753 (1990).
24. Ethier, C.R., Steinman, D.A., Zhang, X., Karpik S.R. and Ojha, M. "Flow waveform effects on end-to-side anastomotic flow patterns", *J. Biomech.*, **31**, pp. 609-617 (1998).
25. He, X. and Ku, D.N. "Pulsatile flow in the human left coronary artery bifurcation: average conditions", *ASME J Biomech Eng.*, **118**, pp. 74-82 (1996).
26. Keynton, R.S., Evancho, M.M., Sims, R.L., Rodway, N.V., Gobin, A. and Rittgers, S.E. "Intimal hyperplasia and wall shear in arterial bypass graft distal anastomoses: An in vivo model study", *ASME J. Biomech Eng.*, **123**, pp. 464-73 (2001).

27. Deng, X., Marois, Y., How, T., Merhi, Y., King, M., Guidoin, R. et al. "Luminal surface concentration of lipoprotein (LDL) and its effect on the wall uptake of cholesterol by canine carotid arteries", *J. Vasc Surg.*, **21**, pp. 135-45 (1995).
28. Xiong, F.L. and Chong, C.K. "A parametric numerical investigation on haemodynamics in distal coronary anastomoses", *Med. Eng. Phys.*, **30**, pp. 311-20 (2007).
29. Fei, D.Y., Thomas, J.D. and Rittgers, S.E. "The effect of angle and flow rate upon haemodynamics in distal vascular graft anastomoses: A numerical model study", *ASME J. Biomech. Eng.*, **116**, pp. 331-36 (1994).
30. Hughes, P.E. and How, T.V. "Effects of geometry and flow division on flow structures in models of the distal end-to-side anastomosis", *J. Biomech.*, **29**, pp. 855-72 (1996).

Biographies

Elnaz Zohravi is a PhD degree student of Mechanical Engineering at Isfahan University of Technology, Iran. She received her BS and MS degrees from the Mechanical Engineering Department at Isfahan University of Technology, Iran, in 2006 and 2009, respectively. Her research interests include biomechanics, cardiovascular modeling, and nano-fluid dynamics.

Ebrahim Shirani is Professor of Mechanical Engineering at Isfahan University of Technology, Iran. He received his BS degree from Sharif University of Technology, Iran, in 1975 and his MS and PhD degrees from Stanford University, USA, in 1977 and 1981, respectively, all in Mechanical Engineering. His research interests include computational fluid dynamics, computational micro and nano-fluid dynamics, turbulence and turbulence modeling and numerical simulation of interfacial flows, turbo machinery and biofluid dynamics. He is author of 12 books, and has published 50 journal and several conference papers. He is also currently faculty member of Foolad Institute of Technology, Fooladshahr, Isfahan, Iran.

Mahmood Reza Sadeghi is faculty member in the Biomedical Engineering Department at the University of Isfahan, Iran. He received his BS degree from Bahonar University of Kerman, Iran, in 1991, his MS degree from Tarbiat Modares University, Tehran, Iran, in 1995, and his PhD degree from Isfahan University of Technology, Iran, in 2013, all in Mechanical Engineering. His research interests include Computational Fluid Dynamics (CFD) in biomechanics, biofluid dynamics, heat and mass transfer in living systems, and Fluid-Structure Interaction (FSI).